Journal of Naval Architecture and Marine Engineering
December, 2024
https://doi.org/10.3329/jname.v21i2.67662 *http://www.banglajol.info*

CHLORIDE-INDUCED CORROSION OF REINFORCING STEEL EMBEDDED IN TERNARY BLENDED CONCRETE

Kazi Naimul Hoque[1*] and Francisco Presuel-Moreno[2]
[1]Department of Naval Architecture and Marine Engineering, Bangladesh University of Engineering and Technology (BUET), Dhaka-1000, Bangladesh. Email: kazinaim@name.buet.ac.bd
[2]Department of Ocean and Mechanical Engineering, Florida Atlantic University (FAU), Dania Beach, Florida, USA. Email: fpresuel@fau.edu

Abstract:

This study investigates the corrosion of steel reinforcement in concrete structures exposed to marine and high humidity environments, focusing on chloride-induced corrosion. Specimens were prepared with two different ternary blended concrete mixes. One mix contains cement replacement of 20% fly ash and 50% slag (termed as T1), while the other contains cement replacement of 20% fly ash and 8% silica fume (termed as T2). On the top surface of the specimens, different size reservoirs were attached, ranging from 5 cm to 15 cm. The reservoirs were filled with NaCl solution with 10% concentration. The electromigration method was employed to accelerate chloride transportation, and corrosion evolution was monitored using electrochemical impedance spectroscopy (EIS) and linear polarization resistance (LPR) techniques for a period of around 900 days. The results showed that the length of the solution reservoir significantly impacts the corrosion current readings. The T2 specimens exhibited lower corrosion current values compared to T1 specimens with similar reservoir lengths, indicating superior corrosion resistance and durability. Electrochemical measurements provide valuable insights into corrosion behavior and mitigation effectiveness. This work emphasizes the importance of the reservoir lengths on different concrete mixes and demonstrates the effectiveness of electrochemical measurements in understanding long-term corrosion performance in reinforced concrete structures.

Keywords: Electromigration, steel rebar, reservoir length, fly ash, slag, silica fume, corrosion current.

1. Introduction

The deterioration of concrete structures reinforced with steel in marine and high humidity environments is primarily attributed to the corrosion of the steel reinforcement (Khatami and Shafei, 2020; Qu et al., 2021; Hajar et al., 2016). Failure to effectively address this issue accelerates the degradation of these reinforced concrete (RC) constructions and leads to a range of interconnected negative consequences. These consequences include a reduction in the service life of RC structures and a decrease in the cross-sectional area of the steel. In the context of RC constructions, corrosion of the steel is often significantly triggered by the penetration of chlorides, known as chloride-induced corrosion. The corrosion rate caused by chloride ingress tends to progress gradually, which complicates the acquisition of timely and actionable information for decision-making. This slow progression delays visible signs of damage, making it difficult to identify early-stage deterioration when interventions are most effective. The collection of adequate data often necessitates long-term monitoring, which requires significant time and resources, thereby hindering prompt insights. Consequently, decisions are often based on limited or overly cautious estimates, increasing the likelihood of costly repairs or unexpected structural failures. Furthermore, the lack of comprehensive research and data pertaining to the initiation and progression of corrosion exacerbates the problem (Castel et al., 2003; Francois and Arliguie, 1998; Otieno et al., 2016; Vidal et al., 2007; Zhang et al., 2009). These studies highlight that significant damage resulting from corrosion in RC structures subjected to natural corrosion mechanisms requires prolonged periods to become evident.

Previous research (Irassar et al., 2000; Hossain and Lachemi, 2004; GjArv, 1995; Hoque, 2016) has provided evidence that the incorporation of cement replacements such as fly ash, silica fume, and blast-furnace slag can yield substantial reductions in the likelihood of steel corrosion and improve the impermeability of concrete. Silica fume, in particular, is widely recognized for significantly enhancing concrete durability. However, fly ash and slag are frequently chosen as alternatives due to their lower workability and cost considerations. According to Torii (Torii, 1995), concrete made with 50% ground granulated blast-furnace slag (GGBS) exhibits a

1813-8535 (Print), 2070-8998 (Online) *Received on July, 2023*

resistance to chloride penetration comparable to that of concrete prepared with 10% silica fume. When these supplementary cementitious materials, such as fly ash, silica fume, and blast-furnace slag, are employed in the form of fine granulates and hydrated, they can partially obstruct pores and voids within the concrete. Consequently, the effective diffusivity of chloride ions and other species is reduced, while the pore size is diminished. It is hypothesized that these actions contribute to an increase in the resistivity of concrete.

In this study, two distinct ternary blended concrete mixes were prepared. The length of the anode was adjusted by modifying the size of the solution reservoir. Electromigration method was employed to accelerate the penetration of chloride ions into the concrete, building upon the findings of previous investigations (Presuel-Moreno et al., 2013). Typically, rebar corrosion initiates after a few weeks or a month. Measurements utilizing electrochemical impedance spectroscopy (EIS) and linear polarization resistance (LPR) techniques were conducted to monitor the corrosion evolution. Parameters such as rebar potential, concrete solution resistance, and corrosion current were measured over a period of approximately 900 days.

2. Experimental Details

2.1 Materials and mix proportions

Two reinforced concrete mixes were prepared and named T1 and T2. Mix T1 contained cement replacement of 20% fly ash and 50% slag, while mix T2 contained cement replacement of 20% fly ash and 8% silica fume. Detailed information regarding the concrete mixtures can be found in Table 1. The specifications for these concrete mixes can be referred to in Appendix 2 of reference (Presuel-Moreno et al., 2018). The segments of the rebars were carefully sized and wire brushed to ensure their proper preparation. Additionally, a hexane solution was used to thoroughly clean the reinforcement, removing any grease or contaminants before the casting process.

Table 1: Concrete mix detail for T1 and T2 specimens

Mix	Cementitious Content (kg/ m^3)	Cement Content (kg/ m^3)	20% FA (kg/ m^3)	8% SF (kg/ m^3)	50% Slag (kg/ m^3)	Fine agg. (kg/ m^3)	Coarse agg. (kg/ m^3)	w/cm ratio
T1	390	117.5	78.3	0	195.2	761	1009	0.41
T2	390	289	70	31	0	790	1046	0.37

The specimens used in this study had dimensions of 30.5 cm x 12.7 cm x 7.6 cm (12 in x 5 in x 3 in). Each of these specimens featured a single rebar section with a radius of 0.47 cm, utilizing #3 rebars. For each concrete mix, five specimens were prepared for T1 and six specimens for T2, all of which had a concrete cover thickness of 0.75 cm (0.3 in). To establish electrical contact for corrosion monitoring, proper drilling and tapping of each rebar were performed.

During the casting process, all specimens were embedded with stainless steel mesh or a titanium mixed metal oxide (TiMMO) mesh on the top surface, which subsequently served as the bottom surface during the experiment. The purpose of the mesh was to accelerate chloride transport. These meshes were positioned at the center of the rebar and had lengths ranging from 5 cm to 15 cm, with a width of approximately 3 cm. After one day, the molds containing the specimens were removed and placed in a fog room for curing.

2.2 Preparation for the experimental setup

After the casting process, the samples were stored at the State Materials Office (SMO) of the Florida Department of Transportation (FDOT) in a highly humid environment for approximately one month. Thereafter, the samples were transferred to the FAU-SeaTech campus, marking the next stage of the experiment. Initially, the samples were kept in a high humidity chamber at FAU-SeaTech before the setup of the solution reservoir.

Once the solution reservoir was installed, the samples were moved to a laboratory setting with a relative humidity of 65% and a temperature of 21°C. A plastic reservoir was securely attached to the top surface of each sample using marine adhesives. It is important to note that the installation of the reservoir took place at least 40

days after the casting of the samples. The reservoir was then filled with a 10% concentration of NaCl solution. The intention was to induce corrosion in various lengths of the rebar.

To prepare for each reservoir filling, the samples were stored in a high humidity environment for a period ranging from 3 to 7 days. The top surface of the solution reservoir was equipped with electrodes composed of either stainless-steel wire mesh or TiMMO mesh, matching the sizes of the embedded meshes. Additionally, a portion of each concrete specimen, approximately one cm in size, was treated with a saturated calcium hydroxide solution. This step was taken to minimize the leaching of chemicals from the concrete by placing the samples on top of a white plastic mesh.

2.3 Electromigration

A power source was employed to establish an electric field between the top and bottom meshes of each specimen, creating a potential hold. The purpose was to drive the chlorides from the solution above the rebar into the concrete, directing them towards the embedded rebar. The negative terminal of the power source was connected to the electrode in the NaCl solution, while the positive terminal was connected to the embedded mesh of each specimen. Fig. 1 provides a visual representation of the electromigration experimental setup.

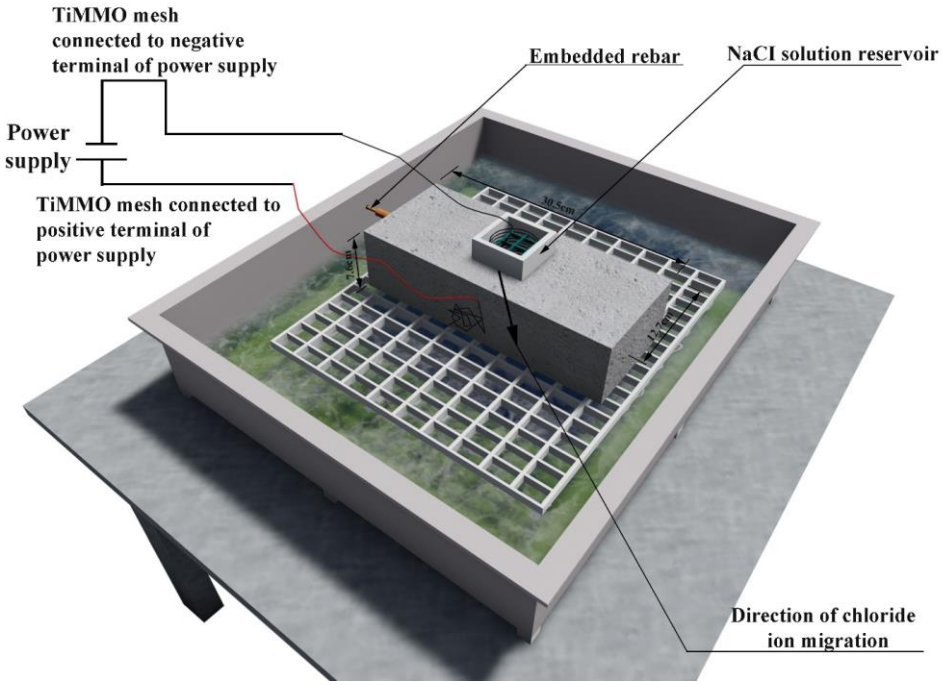

Fig. 1: Experimental setup used for electromigration

The electromigration method was implemented on each specimen. Initially, a 9 V applied potential was utilized. As the rebar potential was assessed in relation to a saturated calomel reference electrode (SCE) while the electric field remained active, a potential higher than +2 V was observed. After 7 days, the applied voltage was reduced to 3 V. The delta potential across a 100-ohm resistor was employed to determine the current magnitude when a specific voltage was applied over several days. When the system was switched off, the rebar potential was measured in relation to a SCE.

Despite not being physically connected, the rebars experienced polarization due to the ionic current driven by the applied electric field. To determine if corrosion had occurred, the rebar potential was monitored for a certain duration, often up to two hours, after disconnecting the system. If the most recent rebar potential measurement indicated the absence of corrosion, the applied potential was restarted. The electromigration process continued until an off-rebar potential, indicating a value of -0.150 Vsce or more negative, was recorded. Previous research

has shown that corrosion typically initiates at a potential of -0.150 Vsce (-0.220 V vs. CSE) (Presuel-Moreno et al., 2013).

Table 2: Single rebar samples made with T1 or T2 mixes

Sample Name	Reservoir Length (cm)	Total Ampere-Hour	Duration (days)
T1(6)	15	0.56	21
T1(7)	5	0.665	30
T1(8)	15	0.565	21
T1(9)	10	0.612	19
T1(10)	5	0.665	30
T2(1)	5	0.578	21
T2(2)	15	0.654	30
T2(3)	5	0.654	30
T2(4)	10	0.536	19
T2(5)	5	0.654	30
T2(11)	15	0.771	21

Table 2 displays the designated labels for each sample, providing important details such as the sample name/ID, reservoir length, and the duration of electromigration. Moreover, the table includes a column indicating the calculated Ampere-hour applied, representing the cumulative values obtained. It is worth noting that each specimen underwent multiple electromigration periods as part of the initial phase of the experiment. To calculate the total Ampere-hour, as detailed in Table 2, the average voltage drop across the resistor was determined. This was done by averaging the initial voltage drop (when the system was active) and the voltage drop recorded just before the system was turned off for a specific period. Using the resistor's value, the average current was then calculated in amperes. This current was multiplied by the total duration (in hours) of the corresponding electromigration period. The Ampere-hour values for all electromigration periods were summed to obtain the total Ampere-hour. During the process, the system was periodically turned off, and the rebar potential was measured at regular intervals relative to a SCE. Additionally, the rebar potential was monitored periodically while the electromigration was active.

3. Monitoring of Corrosion Propagation

During the corrosion propagation stage, the rebar half-cell potential (OCP) was regularly monitored using a SCE (ASTM, 2009). The measurements of solution resistance (Rs) and corrected polarization resistance (Rc) were conducted at least two days after the system had been disconnected. The Rc value was determined by subtracting the solution resistance from the apparent polarization resistance. The EIS test was conducted between the frequencies of 10 kHz and 1 Hz, with the impedance magnitude set at 54.51 Hz for Rs (Kelly et al., 2003). This was done before the LPR measurement (Kelly et al., 2003). The LPR test was conducted from 10 mV below OCP to 1 mV above it. After approximately six months, the LPR measurements were carried out from 8 mV below OCP to the OCP, using either a 0.1 mV/s or 0.05 mV/s scan rate.

During the electromigration period, measurements of the rebar potential, EIS, and LPR were performed, but only after the system had been inactive for a minimum of two days. After the electromigration process was halted, these measurements were carried out once a month. The Rc values obtained from the LPR/EIS readings were subsequently converted to corrosion current (Icorr) since the corroding area was unknown. The determination of Icorr utilized the Stern-Geary equation, specifically Icorr = B/Rp, where Rp represents the polarization resistance (previously defined as Rc), and B is the Stern-Geary coefficient. The value of B ranged from 13 to 52 mV depending on the corrosion condition of the steel (i.e., passive, or active) (Feliu et al., 2007; Gonzalez et al., 2004). For this study, a value of 26 mV was employed.

4. Results and Discussion

4.1 Evolution of Rs, Rc, and rebar potential

In the following figures (Fig. 2 and Fig. 3), the initial day represented as "Day zero," signifies the moment when the solution was introduced into the installed solution reservoir. It does not indicate the age of the specimen. The figure illustrates the progression of corrosion, which is depicted on the right side of the dashed line. The arrow mark following the dashed lines, located to the right of them, represents the period after migration. This period indicates the duration of time after the migration process has occurred. In cases where two black dashed lines are present, the range between them signifies the total duration for which the samples were exposed to electromigration. Inside this range, the blue prisms represent the precisely measured duration during which the electric field was applied, also known as the "system on" period.

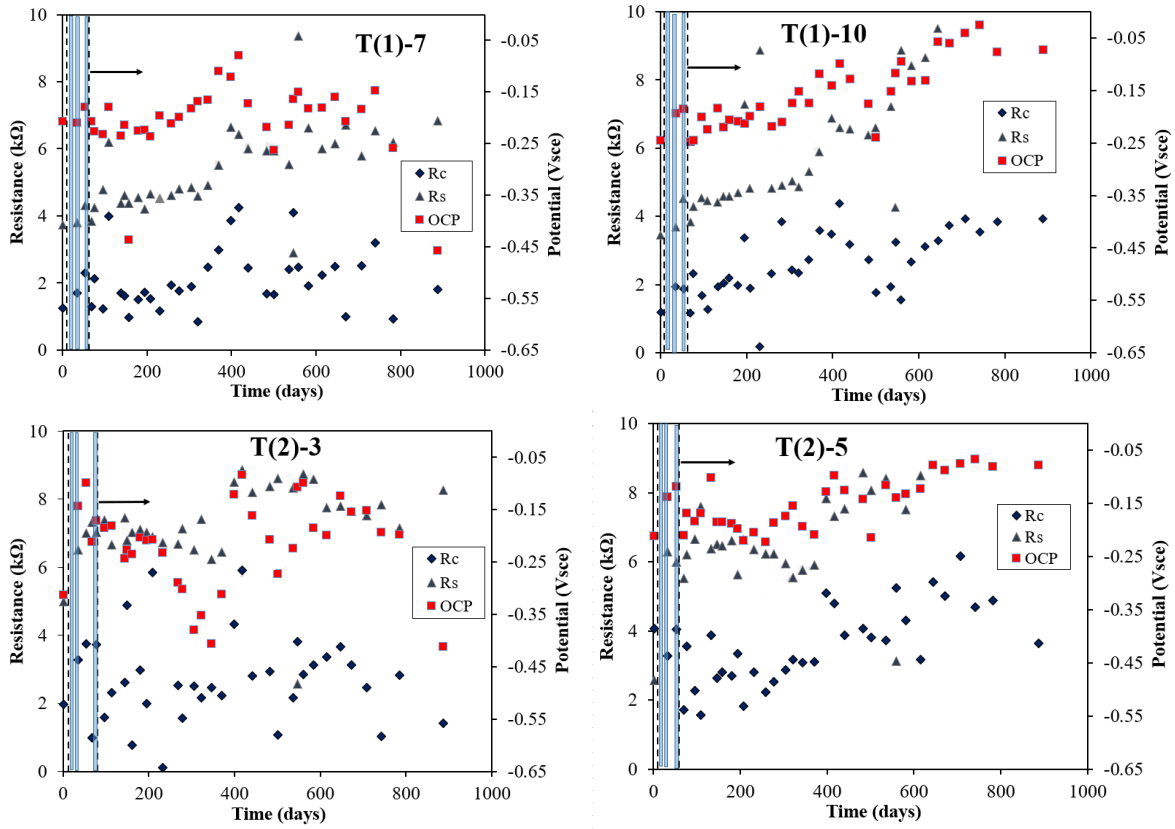

Fig. 2: Rs, Rc, and rebar potential measured on selected rebars under 5 cm reservoir

Fig. 2 provides a visual representation of four plots depicting the evolution of rebar potential, Rs, and Rc for four distinct rebars, namely T1(7), T1(10), T2(3), and T2(5). All these rebars had a solution reservoir size of 5 cm. Interestingly, all these samples required a relatively shorter duration of electromigration, approximately 50 days, to exhibit negative potential values and lower Rc values. In the case of the T1(7) sample, the rebar potential did not undergo significant changes initially. However, as the days progressed, it began to display a fluctuating trend. On the other hand, the T1(10) sample exhibited a different behavior. Despite the increasing trend in Rc values, its rebar potential became more positive over time. For the T2(3) sample, the rebar potential followed a downward trend for approximately 300 days after the electromigration process was discontinued. By day 344, the rebar potential reached a value of -0.406 Vsce. Afterward, the potential started to shift towards a more positive direction, displaying fluctuations as time passed. In contrast, the rebar potential for the T2(5) sample showed a consistently positive trend as the days progressed. Rc values for the T2(5) sample demonstrated an increasing trend, indicating a gradual rise over time. However, the Rc values for the T2(3) sample exhibited a fluctuating pattern as time progressed. It is worth noting the diverse range of rebar potential

values observed. At day 888, the rebar potential values were measured as follows: -0.458 Vsce for T1(7), -0.072 Vsce for T1(10), -0.411 Vsce for T2(3), and -0.079 Vsce for T2(5). These measurements highlight the variations in rebar potential among the different rebars over the given duration.

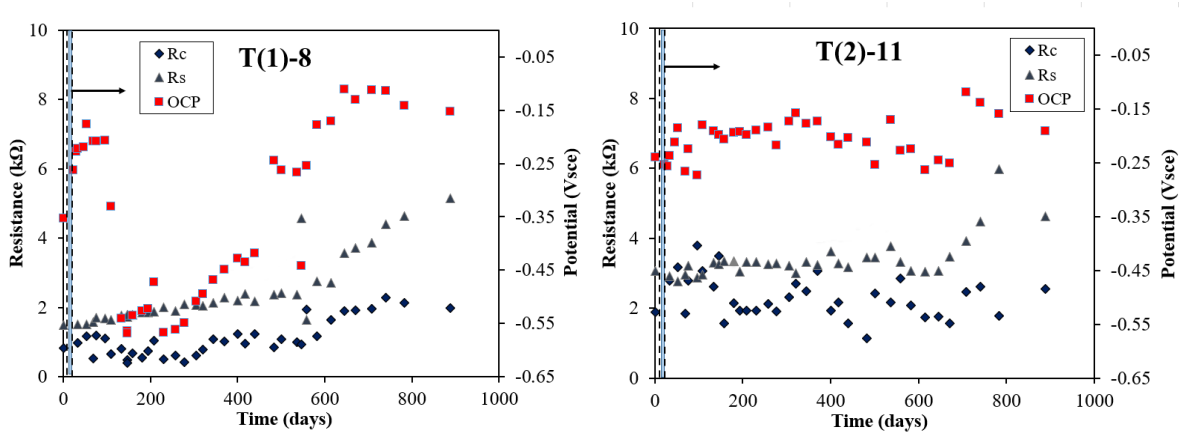

Fig. 3: Rs, Rc, and rebar potential measured on selected rebars under 15 cm reservoir

Fig. 3 presents two plots illustrating the evolution of rebar potential, Rs, and Rc for two distinct rebars, namely T1(8) and T2(11). These rebars had a solution reservoir size of 15 cm. It is worth noting that comparatively less electromigration was required for these samples to exhibit negative potential values and lower Rc values. In the case of the T1(8) sample, a sharp drop in rebar potential was observed after the electromigration process was suspended. By day 147, the rebar potential value reached a value of -0.568 Vsce, indicating a more negative potential. However, as time progressed, the rebar potential displayed a more positive trend. Simultaneously, the Rc values exhibit an upward trend within the range of 0.5-2 kΩ. In contrast, the rebar potential for the T2(11) sample did not undergo significant changes after the electromigration process was discontinued. However, recent rebar potential values showed fluctuations as the days progressed. Similarly, the Rc values for these samples demonstrated a slightly fluctuating trend over time. The variety of rebar potential ranges observed in this study is intriguing. At day 888, the rebar potential values measured were -0.152 Vsce for T1(8) and -0.190 Vsce for T2(11) samples, respectively. References (Presuel-Moreno et al., 2022, 2018; Hoque, 2020; Presuel-Moreno and Hoque, 2019) contains the figures for the other T1 and T2 specimens.

Table 3: Average Rs, Rc, and rebar potential obtained from LPR/EIS readings

Sample Name	Reservoir Length (cm)	Average values obtained from LPR/EIS		
		Rs (kΩ)	Rc (kΩ)	Rebar potential (Vsce)
T1(6)	15	2.03	0.72	-0.471
T1(7)	5	5.31	2.08	-0.206
T1(8)	15	2.41	1.09	-0.340
T1(9)	10	2.59	1.12	-0.389
T1(10)	5	6.67	2.57	-0.159
T2(1)	5	6.41	2.66	-0.318
T2(2)	15	3.15	1.49	-0.277
T2(3)	5	7.25	2.70	-0.216
T2(4)	10	3.96	1.75	-0.337
T2(5)	5	7.49	3.58	-0.152
T2(11)	15	3.39	2.30	-0.206

Table 3 presents the average values of Rs, Rc, and rebar potential obtained from LPR/EIS readings for T1 and T2 single rebar specimens. These averages were calculated using measurements taken over a monitoring period of approximately 900 days. For the T1 specimens, it was observed that the rebars embedded in specimens with a

smaller solution reservoir size of 5 cm exhibited the highest average Rs and Rc values. Conversely, the rebars embedded in specimens with a longer solution reservoir size of 15 cm displayed the lowest average Rs and Rc values. Regarding the T2 specimens, it was found that the rebars embedded in specimens with a smaller solution reservoir of 5 cm had the highest average Rs and Rc values. On the other hand, the rebars embedded in specimens with a longer solution reservoir of 15 cm exhibited the lowest average Rs and Rc values. Across all the specimens, the average rebar potential values were more negative than -0.150 Vsce. Notably, for the rebars embedded in T1 specimens with reservoir lengths of 10 cm and 15 cm, the average rebar potential values were even more negative than -0.338 Vsce. It is important to highlight that any rebar located outside of the concrete, as well as any section of the rebar not directly below the reservoir, affected the measured rebar potential and other readings. In certain cases, the moisture content was excessively high, causing corrosion of the rebar exposed to the air. This phenomenon likely had an impact on the measured Rc values and the rebar potential. Similar observations were reported in these studies (Hoque and Presuel-Moreno, 2024, 2022).

The fluctuations in corrosion potential observed in reinforced concrete specimens arise from variations in corrosion activity across different regions. These fluctuations can be influenced by various factors, including differences in concrete mixes, availability of oxygen, moisture content, and chloride concentration. These factors contribute to localized corrosion, which in turn leads to potential fluctuations. Moreover, changes in the corrosion environment can also contribute to variations in corrosion potential. Factors such as temperature and humidity play a role in influencing the electrochemical reactions occurring at the steel reinforcement, thus giving rise to potential fluctuations. These fluctuations occur as the environmental conditions impact the kinetics of corrosion reactions and modify the electrochemical behavior of the system. Consequently, the observed potential fluctuations reflect the dynamic nature of the corrosion process influenced by these environmental variables.

4.2 Evolution of Icorr

The following figures (Fig. 4 and Fig. 5) showcases the time-dependent evolution of Icorr (corrosion current) as observed through LPR/EIS measurements. It is crucial to understand that the term "day zero" depicted in the plot does not indicate the age of the specimens. Instead, it signifies the specific day when the solution was introduced to the associated solution reservoirs. It should be noted that the filling of the solution reservoirs did not occur simultaneously, resulting in varying durations since the initial fill. The Icorr plots presented in the figure pertain to T1 and T2 mixes. These plots represent the measured values of Icorr obtained through the LPR/EIS method for an approximate duration of 900 days.

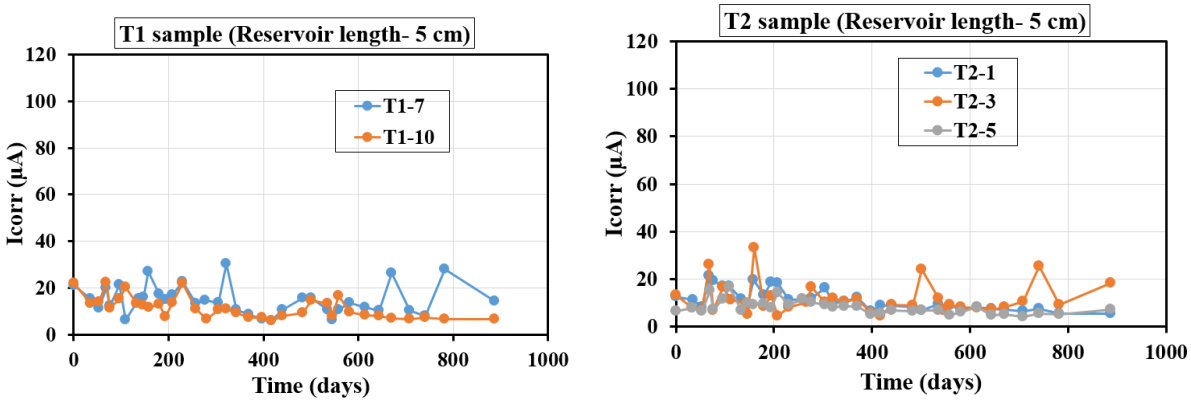

Fig. 4: Icorr vs. time on selected rebars for T1 and T2 samples having 5 cm solution reservoirs

Fig. 4 depicts the progression of Icorr over time, as observed through electrochemical measurements performed on two different sample sets, T1 and T2. The visual representation provides insights into the temporal changes in Icorr for these samples. Each of these samples had a reservoir length of 5 cm. For the T1 sample, the Icorr values for T1-7 exhibited a fluctuating pattern over time, ranging from 6.2 to 30.6 µA. Similarly, the Icorr values for T1-10 displayed a fluctuating trend over time, reaching a peak value on day 231. Subsequently, the Icorr values gradually decreased and remained consistently below 10.0 µA from day 600 to day 900 for T1-10 sample. Throughout the monitoring period, the Icorr values for T1-10 sample ranged from 6.0 to 22.3 µA.

Regarding the T2 sample, the Icorr values for T2-1 and T2-5 samples demonstrated modest fluctuations over time, consistently remaining below 10.0 µA from day 400 to day 900. Specifically, the Icorr values ranged from 5.4 to 21.5 µA for T2-1 sample and 4.2 to 16.7 µA for T2-5 sample, respectively. In contrast, the T2-3 sample exhibited significant fluctuations over time, reaching its peak value on day 159, with Icorr values ranging from 4.4 to 33.2 µA. Fig. 5 shows the time-dependent variation of Icorr for two sample sets, T1 and T2, measured electrochemically, with each sample sets having a 15 cm reservoir length. Furthermore, additional information regarding the evolution of Icorr over time in the remaining T1 and T2 specimens, which possessed reservoirs of various sizes, can be found in these references (Hoque, 2020, Presuel-Moreno et al., 2018).

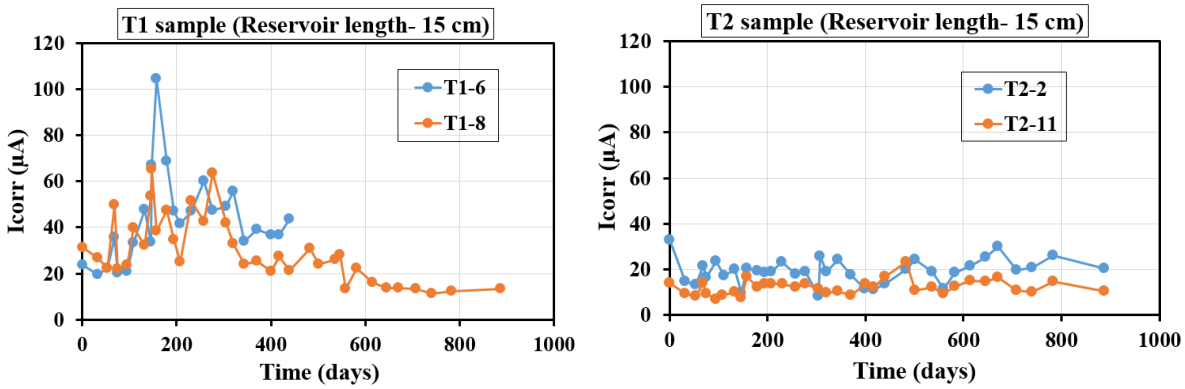

Fig. 5: Icorr vs. time on selected rebars for T1 and T2 samples having 15 cm solution reservoirs

Table 4: Icorr average and STD obtained from LPR/EIS readings

Sample Name	Reservoir Length (cm)	Icorr average (µA)	STD (µA)
T1-7	5	15.1	6.2
T1-10		11.5	4.7
T1-9	10	28.2	11.8
T1-6	15	42.1	18.8
T1-8		28.8	13.3
T2-1	5	11.3	4.6
T2-3		11.6	6.5
T2-5		8.1	3.0
T2-4	10	17.0	7.8
T2-2	15	19.2	5.4
T2-11		12.1	3.3

Table 4 provides comprehensive information on the Icorr average and standard deviation (STD) values obtained from LPR/EIS readings for single rebar specimens cast with T1 and T2 mixes. These measurements were conducted over a monitoring period of approximately 900 days to calculate the averages. In the case of the T1 sample with a reservoir length of 15 cm, the Icorr average and STD values were observed as follows: T1-6 had an average of 42.1 µA with a STD of 18.8 µA, and T1-8 had an average of 28.8 µA with a STD of 13.3 µA. For the T1 sample with a reservoir length of 10 cm, T1-9 had an Icorr average of 28.2 µA with a STD of 11.8 µA. For the T1 sample with a reservoir length of 5 cm, T1-7 had an Icorr average of 15.1 µA with a STD of 6.2 µA, and T1-10 had an Icorr average of 11.5 µA with a STD of 4.7 µA. Similarly, for the T2 sample with a reservoir length of 15 cm, T2-2 had an Icorr average of 19.2 µA with a STD of 5.4 µA, and T2-11 had an Icorr average of 12.1 µA with a STD of 3.3 µA. For the T2 sample with a reservoir length of 10 cm, T2-4 had an Icorr average of 17.0 µA with a STD of 7.8 µA. For the T2 sample with a reservoir length of 5 cm, T2-1 had an Icorr average of 11.3 µA with a STD of 4.6 µA, T2-3 had an Icorr average of 11.6 µA with a STD of 6.5 µA, and T2-5 had an Icorr average of 8.1 µA with a STD of 3.0 µA. It is interesting to note that for the T1 sample, the rebar embedded in T1-6 (reservoir length of 15 cm) exhibited the highest Icorr average value, while T1-10 (reservoir

length of 5 cm) sample had the lowest Icorr average value. In the case of the T2 sample, the rebar in T2-2 (reservoir length of 15 cm) sample had the highest Icorr average reading, while rebar embedded in T2-5 (reservoir length of 5 cm) sample had the lowest Icorr average reading. The Icorr average values for FA samples (with 20% cement replacement by fly ash) ranged from 39.9 to 91.0 µA (Balasubramanian, 2019). These samples, which were vertically installed, were subjected to electromigration techniques to accelerate chloride transport (Balasubramanian, 2019). In this study, the samples were positioned horizontally, and chloride ponds were constructed vertically above the rebar embedded within the specimens. Additionally, it was reported that the Icorr values for T2 specimens ranged from 9.7 to 25.3 µA (Kayali and Zhu, 2005). Furthermore, for concrete mixes containing fly ash as a cement replacement, the Icorr average values were found to be 49.9 µA (Otieno et al., 2016) and 38.5 µA (O'Reilly et al., 2019), respectively.

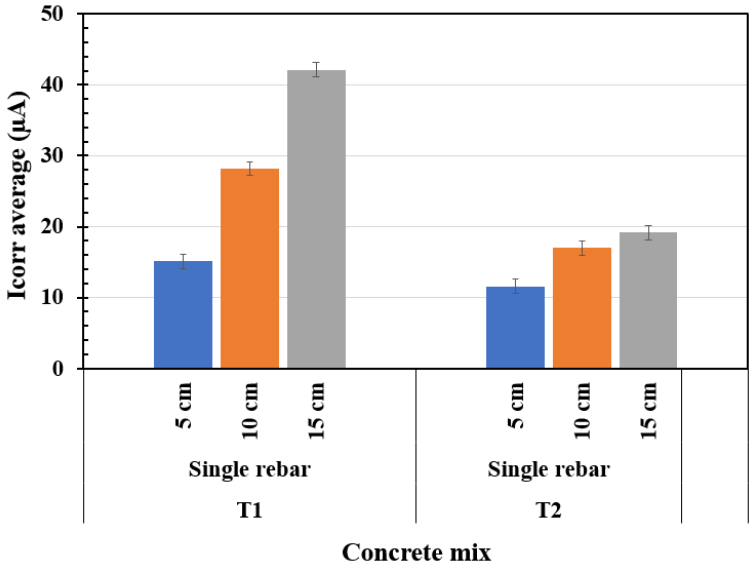

Fig. 6: Variation of Icorr average with length of solution reservoir for T1 and T2 concrete mixes cast with single rebar

The observed variations in Icorr can be attributed to a range of factors encompassing various aspects of the experimental setups. These factors include differences in specimen size, both small and large, leading to variations in the total surface area exposed to the corrosive environment. Discrepancies in the methods used for chloride transport, such as different exposure durations or application techniques, can also contribute to the observed variations. Moreover, variations in the types of admixtures and raw materials employed, differences in the composition of cement mixes, and inconsistencies in the mixed design of concrete specimens can significantly impact Icorr values. The variations in microstructure, which can be influenced by factors like curing conditions and the presence of aggregates, can also contribute to the observed discrepancies. Additionally, differences in the rebar potential, the total ampere-hour applied during testing, and variations in environmental conditions such as oxygen availability, moisture content, and temperature can further affect Icorr values. It is important to consider these diverse experimental parameters and conditions when comparing Icorr results across different research endeavors. These factors play a crucial role in the observed discrepancies and emphasize the need for careful consideration and standardization of experimental protocols to ensure meaningful comparisons and interpretations of Icorr data in corrosion studies.

Fig. 6 presents a summary of the relationship between the Icorr average and the length of the solution reservoir for T1 and T2 concrete mixes. The Icorr average values were obtained using the LPR/EIS method and were derived from readings taken over a monitoring period of approximately 900 days. For both T1 and T2 concrete mixes, the Icorr average increases as the reservoir length increases from 5 cm to 15 cm. The T1 mix exhibits higher Icorr values across all reservoir lengths compared to the T2 mix, indicating a greater corrosion rate for T1 samples under similar conditions. The trend is consistent for both T1 and T2 mixes, with a significant increase in Icorr as the reservoir length reaches 15 cm, showing a clear influence of reservoir length on corrosion activity.

5. General Discussion

The corrosion behavior of reinforced concrete is profoundly influenced by the composition of the concrete mix, reservoir lengths, and environmental conditions. In this study, T1 mixes, incorporating fly ash and slag, generally exhibited better protection against corrosion compared to T2 mixes, which included fly ash and silica fume. The T1 samples typically displayed more negative rebar potential values, indicative of a stable passive layer. In contrast, T2 mixes showed higher variability in rebar potential trends, particularly in shorter reservoirs, highlighting their comparatively lower protective capability under similar conditions. The Rs and Rc values further reinforced the superior performance of T1 mixes in shorter reservoirs, where corrosion initiation was better mitigated.

The reservoir length significantly affected the corrosion parameters across both T1 and T2 mixes. The shorter reservoirs (5 cm) demonstrated higher Rs and Rc values, reducing ionic mobility and limiting corrosion rates. Consequently, Icorr values were lowest in shorter reservoirs, highlighting their ability to reduce corrosion activity. However, as reservoir length increased to 10 cm and 15 cm, both Rc and Rs decreased, signaling enhanced ionic conductivity and moisture content. This led to a notable rise in Icorr values, with longer reservoirs (15 cm) exhibiting the most aggressive corrosion conditions for both T1 and T2 specimens. Similar findings have been documented in previous research conducted by Hoque and collaborators (Hoque et al., 2023). These studies highlighted comparable trends and correlations, further validating the observations reported here.

The environmental conditions such as oxygen availability, chloride concentration, and humidity played a pivotal role in determining corrosion behavior. The fluctuations in rebar potential were closely linked to moisture content and oxygen diffusion, particularly in T2 specimens, where variability was more pronounced. It is noted that higher humidity levels enhanced ionic movement, resulting in lower Rs values and higher Icorr. These conditions were particularly significant in longer reservoirs, emphasizing the dynamic nature of corrosion processes influenced by external factors.

The time-dependent trends in Icorr values revealed differences in the susceptibility of T1 and T2 mixes to corrosion under varying conditions. The T1 specimens showed higher Icorr values in longer reservoirs, suggesting their vulnerability in environments with increased ionic conductivity. On the other hand, T2 mixes exhibited lower Icorr values overall, pointing to the stabilizing effect of silica fume over time. However, T2 mixes also faced challenges in maintaining a stable passive layer, especially under fluctuating environmental conditions.

Therefore, the interplay between concrete mix composition, reservoir length, and environmental factors is critical in determining the durability and corrosion resistance of reinforced concrete. The T1 mixes excel in environments with limited exposure, such as shorter reservoirs, while T2 mixes demonstrate better long-term stability in certain conditions. The adjustment of these factors can improve the durability and efficiency of reinforced concrete structures, making them more resistant to different corrosive conditions. A similar observation was noted in these studies (Kayali and Zhu, 2005; Otieno et al., 2016; O'Reilly et al., 2019; Hoque, 2020). These investigations reported analogous trends, reinforcing the findings presented in this analysis. Each of these studies (Kayali and Zhu, 2005; Otieno et al., 2016; O'Reilly et al., 2019; Hoque, 2020) explored the factors influencing corrosion processes, offering valuable insights that align with the current results.

6. Conclusions

This study employed an accelerated chlorine transport approach to investigate the corrosion behavior of the specimens. Corrosion initiation was observed in all specimens within a few weeks after suspending the electromigration process. The subsequent corrosion propagation was monitored over a period of approximately 900 days. Notably, the length of the solution reservoirs had a significant influence on the corrosion related parameters obtained through electrochemical experiments.

For the rebars embedded in the T1 and T2 concrete mixes, it was observed that the corrosion current values exhibited an increasing trend with the length of the solution reservoir. Comparing specimens with similar reservoir lengths, the corrosion current values were generally higher for the T1 specimens in comparison to the

T2 specimens. This suggests that the specimens prepared with T2 concrete mixes possess greater durability in terms of corrosion resistance when compared to those prepared with T1 concrete mixes.

The utilization of electrochemical measurements in this study allowed for effective monitoring and understanding of the corrosion behavior displayed by the specimens. Through such measurements, researchers can be able to assess the corrosion resistance of the specimens and evaluate the effectiveness of different corrosion mitigation approaches. The examination of corrosion current plots in this study provides valuable insights into the long-term corrosion performance and the efficacy of corrosion mitigation measures employed in the rebars embedded in T1 and T2 concrete mixes.

Acknowledgements

The authors extend their heartfelt gratitude to the Florida Department of Transportation (FDOT) for their assistance with sample preparation. The authors also acknowledge the financial support provided by FDOT and the USDOT through the TriDurLE grant program. The authors sincerely thank Florida Atlantic University (FAU) and the students of the Marine Materials and Corrosion Laboratory at FAU for their hard work in the lab and data collection. The views expressed in this paper are solely those of the authors and do not necessarily reflect the perspectives of FAU, FDOT, or TriDurLE.

References

ASTM C876-09 (2009): Standard test method for corrosion potentials of uncoated reinforcing steel in concrete, in Annual Book of Standards–Section Four Construction, American Society for Testing Materials, West Conshohocken, PA, USA.

Balasubramanian, H. (2019): Initiation and Propagation of Corrosion in Dry Cast Reinforced Concrete Pipes with Environmental Effects. Ph.D. Dissertation, Department of Ocean & Mechanical Engineering, Florida Atlantic University.

Castel, A., Vidal, T., Francois, R., and Arliguie, G. (2003): Influence of steel-concrete interface quality on reinforcement corrosion induced by chlorides. Mag. Concr. Res., vol. 55(2), pp. 151-160. https://doi.org/10.1680/macr.2003.55.2.151

Feliu, V., Gonzalez, J.A., and Feliu, S. (2007): Corrosion estimates from transient response to a potential step. Corrosion Science, vol. 49(8), pp. 3241-3255. https://doi.org/10.1016/j.corsci.2007.03.004

Francois, R., and Arliguie, G, (1998): Influence of service cracking on reinforcement steel corrosion. J. Mater. Civ. Eng., vol. 10(1), pp. 14-20. https://doi.org/10.1061/(ASCE)0899-1561(1998)10:1(14

GjArv, O.E. (1995): Effect of condensed silica fume on steel corrosion in concrete. ACI Mater. J., 92-M60, pp. 591-598.

Gonzalez, J.A., Miranda, J.M., and Feliu, S. (2004): Consideration on the reproducibility of potential and corrosion rate measurements in reinforced concrete. Corrosion Science, 46(10), pp. 2467-2485. https://doi.org/10.1016/j.corsci.2004.02.003

Hajar, H.M., Zulkifli, F., Mohd Sabri, M.G., and Wan Nik, W.B. (2016): Protection against corrosion of aluminum alloy in marine environment by lawsonia inermis. International Journal of Corrosion, Article ID. 4891803. https://doi.org/10.1155/2016/4891803

Hoque, K.N., and Presuel-Moreno, F. (2024): Electromigration-Based Investigation of Corrosion Behaviour in Ternary Blended Reinforced Concrete. International Journal of Structural and Civil Engineering Research, vol. 13(3), pp. 90-95. https://www.ijscer.com/show-188-667-1

Hoque, K.N., Presuel-Moreno, F., and Nazim, M. (2023): Corrosion of carbon steel rebar in binary blended concrete with accelerated chloride transport. Journal of Infrastructure Preservation and Resilience, vol. 4(26), pp. 1-15. https://doi.org/10.1186/s43065-023-00092-7

Hoque, K.N., Presuel-Moreno, F., and Nazim, M. (2023): Accelerated Electromigration Approach to Evaluate Chloride-Induced Corrosion of Steel Rebar Embedded in Concrete. Advances in Materials Science and Engineering, Article ID. 6686519, pp. 1-14. https://doi.org/10.1155/2023/6686519

Hoque, K.N., and Presuel-Moreno, F. (2023): Accelerated Corrosion of Steel Rebar in Concrete by Electromigration: Effect of Reservoir Length and Concrete Mixes. Proceedings of MARTEC 2022. http://dx.doi.org/10.2139/ssrn.4446360

Hoque, K.N., and Presuel-Moreno, F. (2023): Corrosion Propagation of Steel Rebar Embedded in Marine Structures Prepared with Binary Blended Concrete Containing Slag. Proceedings of MARTEC 2022. http://dx.doi.org/10.2139/ssrn.4447455

Hoque, K.N., and Presuel-Moreno, F. (2023): Corrosion Behaviour of Reinforcing Steel Embedded in Fly Ash Concrete. Proceedings of MARTEC 2022. http://dx.doi.org/10.2139/ssrn.4447479
Hoque, K.N., and Presuel-Moreno, F. (2023): Corrosion of Steel Rebar Embedded in Ternary Blended Concrete Exposed to High Humidity Environment. Proceedings of MARTEC 2022. http://dx.doi.org/10.2139/ssrn.4447482
Hoque, K. (2020): Corrosion propagation of reinforcing steel embedded in binary and ternary concrete. Ph.D. Dissertation, Department of Ocean and Mechanical Engineering, Florida Atlantic University (FAU), Boca Raton, Florida, USA.
Hoque, K. N. (2016): Analysis of structural discontinuities in ship hull using finite element method. M.Sc. Thesis, Department of Naval Architecture and Marine Engineering, Bangladesh University of Engineering and Technology (BUET), Dhaka, Bangladesh.
Hossain, K.M.A., and Lachemi, M. (2004): Corrosion resistance and chloride diffusivity of volcanic ash blended cement mortar. Cem. Concr. Res., vol. 34 (4), pp. 695-702. https://doi.org/10.1016/j.cemconres.2003.10.021
Irassar, E.F., Gonzalez, M., and Rahhal, V. (2000): Sulphate resistance of type V cements with limestone filler and natural pozzolana. Cem. Concr. Compos., vol. 22, pp. 361-368. https://doi.org/10.1016/S0958-9465(00)00019-6
Kayali, O., and Zhu, B. (2005): Chloride induced reinforcement corrosion in lightweight aggregate high-strength fly ash concrete. Construction and Building Materials, vol. 19, pp. 327-336. https://doi.org/10.1016/j.conbuildmat.2004.07.003
Kelly, R.G., Scully, J.R., Shoesmith, D.W., and Buchheit, R.G. (2003): Electrochemical Techniques in Corrosion Science and Engineering. Maecel Dekker, Inc., New York, NY, USA. https://doi.org/10.1201/9780203909133
Khatami, D., and Shafei, B. (2020): Impact of Climate Conditions on Deteriorating Reinforced Concrete Bridges in the US Midwest Region. Journal of Performance of Constructed Facilities, vol. 35(1), pp. 1-26. https://doi.org/10.1061/(ASCE)CF.1943-5509.0001528
O'Reilly, M., Omid, F., and Darwin, D. (2019): Effect of Supplementary Cementitious Materials on Chloride Threshold and Corrosion Rate of Reinforcement. ACI Materials Journal, Title No. 116-M12, pp. 125-133.
Otieno, M., Beushausen, H., and Alexander, M. (2016): Chloride-induced corrosion of steel in cracked concrete-part I: experimental studies under accelerated and natural marine environments. Cem. Concr. Res., vol. 79, pp. 373-385. https://doi.org/10.1016/j.cemconres.2015.08.009
Presuel-Moreno, F., Hoque, K., and Rosa-Pagan, A. (2022): Corrosion propagation monitoring using galvanostatic pulse on reinforced concrete legacy samples. 2020-FAU-02 Final Report for National University Transportation Center TriDurLE.
Presuel-Moreno, F., and Hoque, K., (2019): Corrosion propagation of carbon steel rebar embedded in concrete. Corrosion 2019, Nashville, Tennessee, USA.
Presuel-Moreno, F., Nazim, M. Tang, F., Hoque, K., and Bencosme, R. (2018): Corrosion Propagation of Carbon Steel Rebars in High Performance Concrete. BDV27-977-08 Final Report for FDOT.
Presuel-Moreno, F., Balasubramanian, H., and Wu, Y.-Y. (2013): Corrosion of reinforced concrete pipes: an accelerated approach. Corrosion 2013, paper no. C2013-0002551, Houston, TX: NACE.
Qu, F., Li, W., Dong, W., Tam, V.W.Y., and Yu, T. (2021): Durability deterioration of concrete under marine environment from material to structure: A critical review. Journal of Building Engineering, vol. 35,102074. https://doi.org/10.1016/j.jobe.2020.102074
Torii, K., Sasatani, T., and Kawamura, M. (1995): Effects of fly ash, blast furnace slag, and silica fume on resistance of mortar to calcium chloride attack. Proceedings of Fifth International Conference on Fly Ash, Silica Fume, Slag, and Natural Pozzolans in Concrete, American Concrete Institute, SP-153, vol. 2, pp. 931-949.
Vidal, T., Castel, A., and Francois, R. (2007): Corrosion process and structural performance of a 17-year-old reinforced concrete beam stored in chloride environment. Cem. Concr. Res., vol. 37(11), pp. 1551-1561. https://doi.org/10.1016/j.cemconres.2007.08.004
Zhang, R., Castel, A., and Francois, R. (2009): Serviceability limit state criteria based on steel-concrete bond loss for corroded reinforced concrete in chloride environment. Mater. Struct., vol. 42(10), pp. 1407-1421. https://doi.org/10.1617/s11527-008-9460